Open Access

Earth System
Science
Data

Discussions

A High-Accuracy Rainfall Dataset by Merging Multi-Satellites and Dense Gauges over Southern Tibetan Plateau for 2014-2019 Warm Seasons

Kunbiao Li[1], Fuqiang Tian[1], Mohd Yawar Ali Khan[2], Ran Xu[1], Zhihua He[3], Long Yang[4], Hui Lu[5], Yingzhao Ma[6]

[1] Department of Hydraulic Engineering, Tsinghua University, Beijing, China

[2] Department of Hydrogeology, King Abdul-Aziz University, Jeddah, Saudi Arabia

[3] Centre for Hydrology, University of Saskatchewan, Saskatoon, SK S7N 5C8, Canada

[4] School of Geography and Ocean Science, Nanjing University, Nanjing, China

[5] Department of Earth System Science, Tsinghua University, Beijing, China

[6] Department of Civil & Environment Engineering, Colorado State University, FT COLLINS, CO, USA

Correspondence: Fuqiang Tian (tianfq@mail.tsinghua.edu.cn)

1

2

3

4

5

6

7

8

9

10

11

12

13

14

15

16

Abstract

Tibetan Plateau (TP) is well known as the Asia's water tower from where many large rivers originate. However, due to complex spatial variability of climate and topography, there is still a lack of high-quality rainfall dataset for hydrological modelling and flood prediction. This study, therefore, aims to establish a high-accuracy daily rainfall product through merging rainfall estimates from three satellites, i.e., GPM-IMERG, GSMaP, and CMORPH, based on the likelihood measurements of a high-density rainfall gauge network. The new merged daily rainfall dataset with a spatial resolution of 0.1°, focuses on warm seasons (June 10th - October 31st) from 2014 to 2019. Statistical evaluation indicated that the new dataset outperforms the raw satellite estimates, especially in terms of rainfall accumulation and the detection of ground-based rainfall events. Hydrological evaluation in the Yarlung Zangbo River Basin demonstrated high performance of the merged rainfall dataset in providing accurate and robust forcings for streamflow simulations. The new rainfall dataset additionally shows superiority to several other products of similar types, including MSWEP and CHIRPS. This new rainfall dataset is publicly accessible at https://doi.org/10.11888/Hydro.tpdc.271303 (Li et al.,2021).

1. Introduction

Precipitation, linking atmospheric and hydrological processes, serves as a crucial component of the water cycle (Eltahir & Bras, 1996; Trenberth et al., 2003). Gridded precipitation datasets become more and more popular with the advent of satellite precipitation measurement. Most famous satellite gridded precipitation datasets include Tropical Rainfall Measuring Mission (TRMM) (Huffman et al., 2007) and its successor the Integrated Multi-satellite Retrievals for Global Precipitation Measurement mission (GPM-IMERG) (Hou et al., 2014), the Global Satellite Mapping of Precipitation

42   (GSMaP) (Ushio et al., 2009), the Climate Prediction Centre (CPC) MORPHing

43   technique (CMORPH) (Joyce et al., 2004), etc. These products have been successfully

44   applied in various hydrometeorological studies and water resources management

45   practices (Kidd, C., & Levizzani, V., 2011; Jiang et al., 2012; Tong et al., 2014; Yang et

46   al., 2015; Sun et al., 2016; Wang et al., 2017).

47   However, all existing precipitation datasets show insufficient accuracy in high

48   mountainous regions (Yilmaz et al., 2016; Derin et al., 2018; Derin et al., 2019;

49   Anagnostou & Zhang, 2019), which hinders our understanding of climate and

50   hydrological processes over these areas. This can be attributed to the complex physical

51   nature of electromagnetic transmission and precipitation forming processes (Hong et

52   al., 2007; Bitew & Gebremichael 2010; Dinku et al., 2010), and harsh environments in

53   high mountains that lead to very limited deployment of in-situ rain gauges with

54   insufficient representation of ground observations for training satellite-based

55   precipitation retrieval algorithms. For instance, the Tibetan Plateau (TP) as the roof of

56   the world is surrounded by imposing mountain ranges with an average elevation

57   exceeding 4000 m. It generates several large rivers in Asia and provides invaluable

58   freshwater resources for more than 1.4 billion people living downstream (Immerzeel et

59   al., 2010). However, this vast plateau has very limited number of precipitation gauges

60   across its 2.5 million km^2 area. The precipitation gauge network operated by China

61   Meteorological Agency (CMA) contains only 86 gauges over the entire TP (Figure 1).

62   These gauges are essential to correct satellite precipitation datasets. For example, GPM-

63   IMERG 'Final' Run dataset uses Global Precipitation Climatology Centre (GPCC)

64   database, GSMap_Gauge and CMORPH use NOAA Climate Prediction Centre (CPC)

65   database. Although both GPCC and CPC databases received data through Global

66   Telecommunication System (GTS), only part of the above-mentioned gauges in TP

67   were utilized (Xie et al., 2007; Becker 2013). Previous evaluations over the TP

68   indicated that most products present dependence on topography to varying degrees, and

69   products adjusted by gauge observations shows better performance than satellite-only

Earth System
Open Access
Science
Data
Discussions

70   products (Gao et al.,2013; Lu et al., 2018). Therefore, a better spatial coverage of rain

71   gauges is critical to correct satellite products in high mountains.

72   In 2014, the Ministry of Water Resources of China (MWR) launched the flash

73   flood monitoring and alarming campaign. A large number of rain gauges is now

74   accessible over the TP, especially in the southern TP. There are 440 new rain gauges,

75   and are available since 2014, independent of the existing CMA precipitation gauge

76   network (Figure 1). These gauges provide measurements of precipitation in liquid phase

77   (i.e., rainfall) at event time scale. A couple of recent studies have demonstrated the

78   utility of this rain gauge network (Xu et al., 2017; He et al., 2017; Tian et al., 2018;

79   Wang et al., 2020). For instance, Xu et al. (2017) evaluated the performance of TRMM

80   and GPM and the dependence on topography and rainfall intensity based on the network.

81   Their results demonstrated that the data quality of this dense gauge network is strictly

82   controlled, serving as the currently highest gauge dense for satellite product evaluation

83   on TP. Wang et al. (2020) used the gauge data to validate their reproduced precipitation

84   dataset. However, there is not a merging product that assimilate the observations from

85   this dense rain gauge network. This is apparently a unique opportunity to improve the

86   performance of existing satellite-based precipitation datasets for its highest density and

87   quality.

88   This study aims to provide a high-accuracy rainfall dataset by merging all

89   available ground gauges and three good-quality satellite precipitation datasets over the

90   southern TP for the warm seasons (June 10th - October 31st) from 2014 to 2019. The

91   remainder of this paper is organized as follows: Section 2 describes the study area and

92   the source data. Section 3 provides details of the data merging method and the methods

93   adopted to evaluate the quality of dataset. Results are presented in Section 4. The data

94   availability and summary are provided in Section 5 and Section 6, respectively.

2. Study Area and Source Data

2.1. Southern Tibetan Plateau

Tibetan Plateau, known as the Asian water tower, borders India, Myanmar, Bhutan and Nepal to the south and Pakistan to the west. Various climate systems affect the plateau, including westerly winds in winter and the Indian monsoon in summer (Yao et al., 2012). Many Asian large rivers originate from this vast area, including the Yellow River, the Yangtze River, the Yarlung Zangbo River (YZR), Jinsha River (JR), Lancang River (LR), Salwen River (SR), Irrawaddy River (IR), Ganges River (GR), and Indus River (IDR). This study is focused on the southern part of TP (Figure 1), including the upper YZR Basin (YZRB) as a major basin.
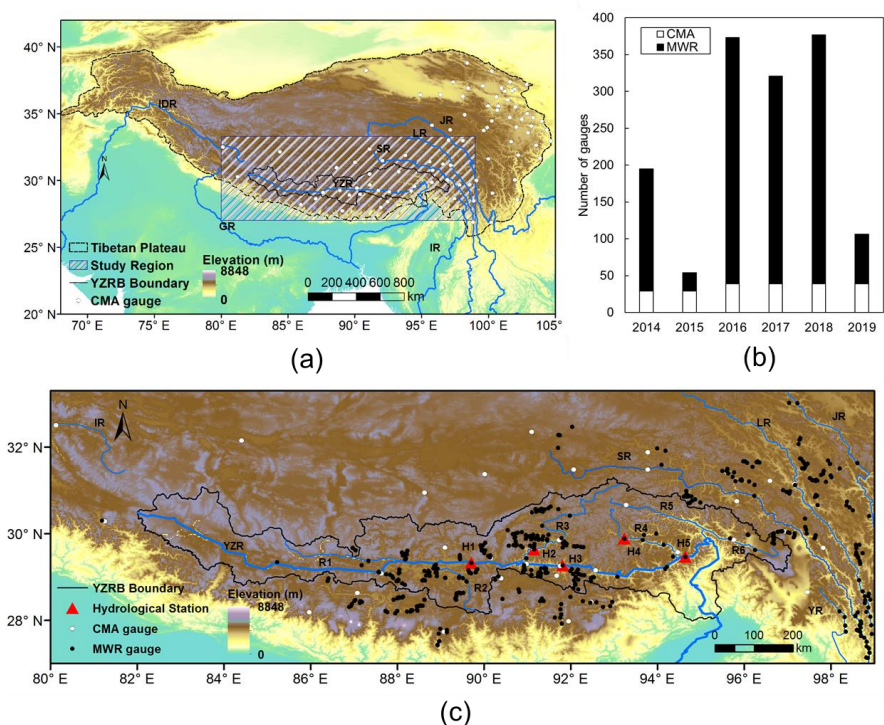

Figure 1. (a) The location and topography of the TP and the spatial distributions of CMA gauges. (b) Numbers of ground gauges installed by CMA and MWR in southern TP during 2014-2019, (c)

5

108   Locations of CMA and MWR rain gauges and main hydrological stations in southern TP. The names

109   of hydrological stations are labelled as H1-Yangcun, H2-Lhasa, H3-Nugesha, H4-Gongbujiangda,

110   H5-Nuxia. The names of tributary rivers are labelled as R1-Duoxiong Zangbo, R2-Nianchu River,

111   R3-Lhasa River, R4-Niyang River, R5-Yigong Zangbo, R6-Parlung Zangbo.

2.2. Ground gauged rainfall

113   We combined two rain gauge networks managed by MWR and CMA to obtain a

114   high-quality ground reference dataset up to date. The number of rain gauge is presented

115   in Figure 1b, and varies across different years. The spatial distribution of all gauges is

116   presented in Figure 1c. The gauges are mainly located in the middle reaches of YZRB

117   and the east part of the study area. Despite the high density, we can see these rain gauges

118   are not evenly distributed across the space. This makes satellite rainfall products over

119   varying altitudes and aspects important. Daily rainfall observations during the warm

120   seasons of 2014-2019 were accumulated from the original event scale measurements.

121   Total number of the CMA and MWR gauges ranges from 53 in 2015 to 377 in 2018,

122   forming the densest rain gauge network up till now.

123   The CMA gauge data has been widely demonstrated as reliable and accurate in

124   previous studies (Zhai et al., 2005; Su et al., 2020; He et al., 2020). Gauge data used in

125   this study has been manufactured under strict quality control procedures, including (1)

126   internal consistency check, (2) extreme values check (0~85mm/h), and (3) spatial

127   consistency check (Ren et al., 2010). Rain gauges with erroneous values (e.g.

128   enormously large values) were discarded from the entire records.

2.3. Satellite Precipitation Datasets

130   Three satellite precipitation products were chosen for the data merging procedure

131   (Lu et al., 2019; Derin et al., 2019; Tang et al., 2020), including GPM-IMERG 'Final'

132   run (here after referred to as IMERG) from the National Aeronautics and Space

133   Administration (NASA) (https://disc.gsfc.nasa.gov/), the GSMaP_Gauge (here after

134 referred to as GSMaP) from Japan Aerospace Exploration Agency (JAXA)

135 (http://sharaku.eorc.jaxa.jp) and the CMORPH v1.0 from NOAA CPC

136 (ftp://ftp.cpc.ncep.noaa.gov/precip/CMORPH_V1.0/). Spatial resolutions and temporal

137 frequency of the satellite datasets are listed in Table 2. To be consistent, IMERG and

138 GSMaP data were accumulated to daily scale (08:00-08:00 of local time, i.e. UTC+8)

139 and CMORPH was bilinearly interpolated to the grid resolution of 0.1°.

140   The merged dataset was further compared with two popular merged rainfall

141 datasets of Climate Hazards Group InfraRed Precipitation with Stations (CHIRPS)

142 (Funk et al., 2015) and Multi-Source Weighted-Ensemble Precipitation (MSWEP)

143 (Beck et al., 2019). CHIRPS was originated by merging CHPClim, thermal infrared,

144 TRMM3B42, NOAA CFSv2 precipitation data, and ground observation precipitation

145 data. MSWEP was merged from multiple datasets including CPC, GPCC, CMORPH,

146 GSMaP-MVK, GPM-IMERG, ERA5, and JRA-55. CHIRPS and MSWEP showed

147 great potentials in rainfall estimates in previous studies (Liu et al., 2019).

148   Table 2. Multiple satellite precipitation datasets used in this study.

Datasets	Resolution	Frequency	Source	Reference
GPM IMERG	0.1 °x 0.1 °	0.5 hourly	NASA	(Hou et al., 2014)
GSMaP_Gauge	0.1 °x 0.1 °	1 hourly	JAXA	(Ushio et al., 2009)
CMORPH v1.0	0.25 °x 0.25 °	daily	CPC	(Joyce et al., 2004)
CHIRPS v2.0	0.25 °x 0.25 °	daily	USGS and CHC	(Funk et al., 2015)
MSWEP v2	0.1 °x 0.1 °	3 hourly	-	(Beck et al., 2019)

149 **3. Methodology**

150   We used the Dynamic Bayesian Model Averaging (DBMA) method (Ma et al.,

151 2017) to merge the satellite datasets with in-situ rain gauges. To evaluate the quality of

152 the new dataset, we carried out statistical and hydrological evaluations and comparisons

153 with CHIRPS and MSWEP in southern TP.

154 **3.1. Dynamic Bayesian Model Averaging method**

155   The Dynamic Bayesian Model Averaging (DBMA) method developed by Ma et

156 al. (2018) was utilized in this work. A flow chart of the merging method is shown in

157 Figure 2. In the first step, a training dataset was formed by selecting samples from the

158 ground gauged data and three original satellite datasets. The training period was set as

159 40 days. Increasing the length of the training period did not lead to obvious

160 improvement of the merging method (Ma et al., 2018). In the second step, the training

161 dataset was transformed by the Box-Cox Gaussian distribution, and the optimal weights

162 for each of the original satellite datasets on a specific grid where a ground gauge is

163 located on each training day were estimated by a logarithmic likelihood equation and

164 the optimal expectation algorithm. In the third step, an ordinary Kriging interpolation

165 method was applied to spatially interpolate the daily weights onto grids with no gauges.

166 Finally, posterior spatiotemporal weights were used to obtain the final merged rainfall

167 dataset. The DBMA-merged data has been proved in Ma et al. (2017) to outperform

168 original satellite data during 2007-2012 over TP.
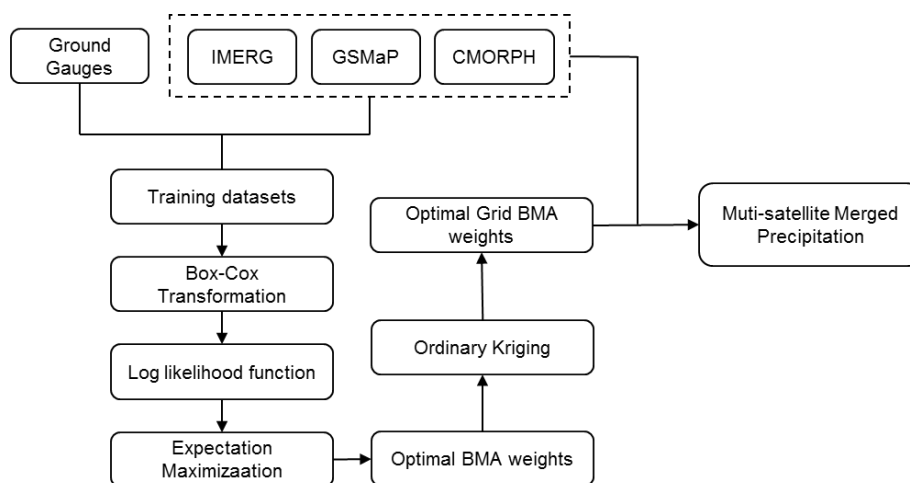
169

170   Figure 2. Flowchart of the DBMA merging method (adapted from Ma et al., 2018).

171   For statistical evaluation of the merged data against ground gauges, around 85%

172 of the gauges were randomly selected to form a training gauge set for the merging

173   approach in each year during 2014-2019, and the remaining 15% were used for test.

174   Table 1 lists the numbers of training and test gauges in each of the warm seasons. The

175   spatial distributions of gauges in each year are presented in Figure S1. Data from all

176   gauges were involved in the training procedure of the final released version of the

177   merged data.

178   Table 1. Number of rain gauges for training and test in 2014-2019.

Year	Total number of rain gauges	Number of training gauges	Number of test gauges
2014	195	166	29
2015	54	46	8
2016	373	317	56
2017	321	273	48
2018	377	320	57
2019	106	90	16

179   **3.2. Statistical Evaluation**

180   Performance of the multiple datasets were statistically evaluated by comparing

181   with ground observations on the corresponding statelite grids. Relative bias (RB) and

182   normalized root mean square error (RMSE) were adopted to measure the amount

183   difference between the gridded rainfall and the gauged rainfall. Correlation Coefficient

184   (CC) was used to evaluate the consistency between satellite estimates and gauge

185   observations. The skill of rainfall data on detecting rainfall occurrence (rainfall events

186   higher than zero) was evaluated through a set of metrics (similarly to Wilks, 2006): i.e.

187   the probability of detection (POD) assessing how good the multiple rainfall datasets are

188   at detecting the occurrence of rainfall, false alarm ratio (FAR) measuring how often the

189   gridded rainfall datasets detect rainfall when there actually is not rainfall, and critical

190   success index (CSI) measuring the ratio of rainfall events that are correctly detected by

191   the gridded datasets to the total number of observed or detected events. Equations for

192   the above metrics are shown in Table 2.

193   Table 2. Statistical indices that were used to assess the performance of the gridded rainfall

Open Access

Earth System
Science
Data

Discussions

194   datasets.

Statistical Indicators	Equation	Optimal Value	Equation number
Relative Bias (RB)	$Bias = \dfrac{\sum_{i=1}^{n}(S_i - G_i)}{\sum_{i=1}^{n} G_i}$	0	(1)
Correlation Coefficient (CC)	$CC = \dfrac{[\sum_{i=1}^{n}(S_i - \bar{S}) \cdot (G_i - \bar{G})]^2}{\sum_{i=1}^{n}(S_i - \bar{S})^2 \cdot \sum_{i=1}^{n}(G_i - \bar{G})^2}$	1	(2)
Root Mean Square Error (RMSE)	$RMSE = \sqrt{\dfrac{1}{n}\sum_{i=1}^{n}(S_i - G_i)^2}$	0	(3)
Probability of Detection (POD)	$POD = \dfrac{a}{a + c}$	1	(4)
False Alarm Ratio (FAR)	$FAR = \dfrac{b}{a + b}$	0	(5)
Critical success index (CSI)	$CSI = \dfrac{a}{a + b + c}$	1	(6)

195   For the equations listed in Table 2, n is the total number of gridded product data

196   and gauge observation data; i is the ith of satellite product data and gauge

197   observation data; G_i means gauge observation and $\bar{G}$ is the average of gauge

198   observation. S_i and $\bar{S}$ are gridded estimates and their average, respectively. a

199   represents hit (i.e., event was detected to occur and observed to occur), b represents

200   false alarm (i.e., event was detected to occur but not observed to occur), and c

201   represents miss (i.e., event was not detected to occur but observed to occur).

202   Triple Collocation (TC) technique provides a platform for quantifying the root

203   mean square errors of three products that estimate the same geophysical variable

204   (Stoffelen, 1998). Roebeling et al. (2012) successfully applied the TC technique to

205   estimate errors of three rainfall products across Europe. An extended Triple Collocation

206   (ETC) introduced in Kaighin et al. (2014), which is able to estimate errors and

207   correlation coefficients with respect to an unknown target was used in this study to

208   compare the performance of the DBMA-merged data and two previous merged datasets

209   of CHIRPS and MSWEP.

3.3. Hydrological Evaluation

In addition to the statistical assessments against rain gauges, hydrological assessment was used as a tool to test the performance of merged rainfall datasets on forcing hydrological modelling in the study area (similarly see Yong et al, 2012; Xue et al, 2013; Yong et al, 2014; Li et al, 2014). In this section, a semi-distributed hydrological model developed by Tian (2006), namely Tsinghua Hydrological Model based on Representative Elementary Watershed (THREW), was adopted for the hydrological assessment of rainfall datasets in the YZRB. YZRB has a drainage area of approximately 240,480 km^2 within China's boarder. The basin elevation ranges from 143 to 7,261 m, with an average of around 4,600 m. YZR is one of the most important transboundary rivers in South Asia and the highest river in the world, which is characterized by a dynamic fluvial regime with exceptional physiographic setting spreading along the eastern Himalayan region (Goswami, 1985). Due to complex terrain and strongly varying elevation, the YZRB is under control of a variety of climate systems, such as the semi-arid plateau climate prevailing in the upper and middle reaches, and the mountainous subtropical and tropical climates prevailing in the lower reaches. In the cold upper reaches, the mean annual rainfall is less than 300 mm. In the warm middle reaches, the mean annual rainfall falls between 300 mm and 600 mm.

The whole basin area above the Nuxia hydrological station was divided into 63 Representative Elementary Watersheds (REWs). Model parameters were calibrated by daily discharges measured at the Nuxia station. The calibration period is scheduled to run in the warm seasons from June 10th to October 31st in 2014- 2017, encompassing a period length of 576 days. The validation period includes two warm seasons in 2018 and 2019 with a total duration of 288 days. Descriptions of the calibrated model parameters can be found in Table 3. An automatic algorithm pySOT developed by D. Eriksson et al (2019) was used to optimize the parameter values based on an objective-function of *NSE* (Nash and Sutcliffe, 1970) in Eq. 7. To conduct a continuous

237 hydrological simulation in the study period, the datasets of daily grid-based

238 precipitation over China (Zhao et al., 2014) were used as model inputs in the non-warm

239 seasons when merged rainfall is not available.

240

Table 3. Calibrated parameters of the THREW model.

Symbol	Description	Unit	Value Range
kv	Fraction of potential transpiration rate over potential evaporation	-	0.001-0.8
n^t	Manning roughness coefficient for hillslope	-	0.0001-0.2
$GaIFL$	Spatial heterogeneous coefficient for infiltration capacity	-	0.0001-0.7
$GaEFL$	Spatial heterogeneous coefficient for exfiltration capacity	-	0.0001-0.7
$GaETL$	Spatial heterogeneous coefficient for evapotranspiration capacity	-	0.0001-0.7
WM	Tensor water storage capacity	cm	0.1-10
B	Shape coefficient to calculate the saturation excess runoff area	-	0.01-1
$Gaus$	Coefficient representing spatial heterogeneity of exchange term between t-zone and r-zone	-	0.001-10
KKA	Exponential coefficient to calculate subsurface flow	-	0.01-6
KKD	Linear coefficient to calculate subsurface flow	-	0.001-0.5
MM	Snow melting degree-day factor	mm/day	0.001-10
MMG	Ice melting degree-day factor	mm/day	0.001-10
$C1+C2$	Muskingum parameter	-	0.0001-1
$C1/(C1+C2)$	Muskingum parameter	-	0.0001-1

$$NSE = 1 - \frac{\sum_{n=1}^{N}(Q_{obs}^n - Q_{sim}^n)^2}{\sum_{n=1}^{N}(Q_{obs}^n - \bar{Q}_{obs})^2} \qquad (7)$$

241 where, N is the total number of days in the evaluation period, Q_{obs}^n and Q_{sim}^n

242 represent the observed and simulated runoff on the nth day, respectively. $\bar{Q}_{obs}$

243 represents the average of observed runoff in the evaluation period.

Earth System
Science
Data

4. Results and Discussions

4.1. Spatiotemporal Patterns

Based on the merging method, a new daily rainfall dataset with spatial resolution of 0.1°×0.1° in the warm seasons from June 10th to October 31st (144 days in each year) in 2014-2019 (864 days in six years) was generated. Figure 3 presents the spatial pattern of the mean rainfall over the six warm seasons of the merged data in southern TP. It is shown that extremely high summer rainfall centres concentrate in the south-eastern and south-western of the study area where is known as a world-famous heavy rainfall centre (see Biskop et al., 2015; Bookhagen & Burbank, 2006; Kumar et al., 2010).
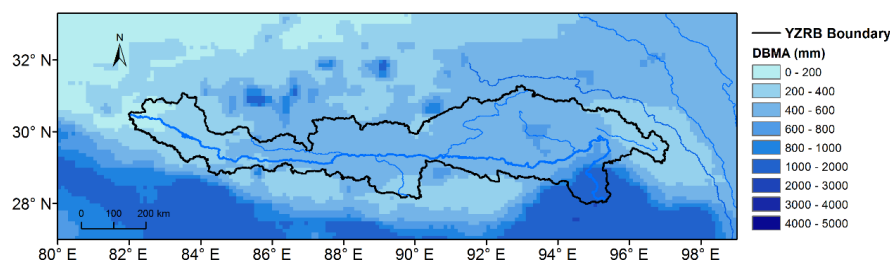
Figure 3. Spatial pattern of mean rainfall over six warm seasons in 2014-2019 of the DBMA-merged data in southern TP.

In addition, Figure 4 compares the time series of average daily weight and rainfall over the YZRB basin derived from the DBMA-merged data and the original satellite datasets. As expected, the DBMA-merged daily rainfall in general fall in the envelope ranges of the three satellite datasets. Merged data is closer to CMORPH in June, September and October, while showing equal closeness to all the three source satellite data in July and August. It indicates that CMORPH is closer to the in-situ gauges than IMERG at basin scale when rainfall value is small, especially for light rainfall events smaller than 2 mm, but this difference tends to be small for heavy rainfall events.
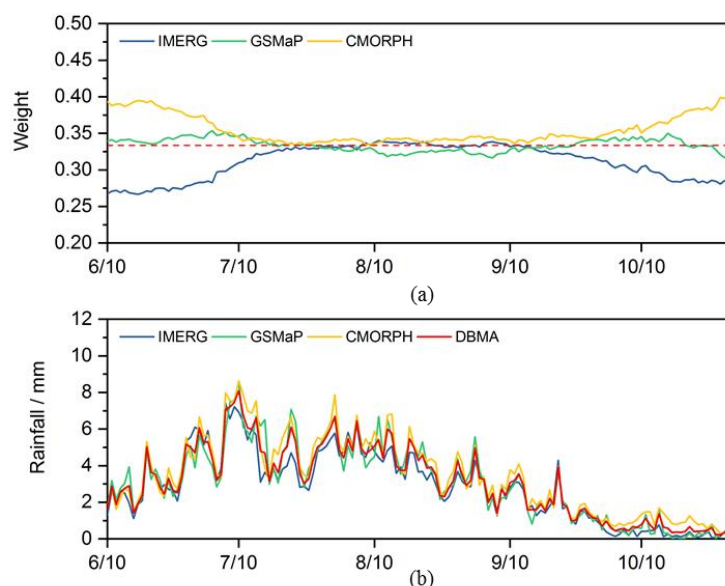
13

Figure 4. Seasonal variations in basin-averaged (a) weights and (b) rainfall estimates of the multiyear daily values of IMERG, GSMaP, CMORPH and DBMA.

4.2. Statistical Evaluation

Figure 5 shows the statistical evaluation of the merged and original datasets in the warm seasons. The statistical indices were calculated for three gauge groups including the training gauges, the test gauges and all gauges at different elevation bands. The datasets in general presented comparable performance for the training and test gauge groups, indicating that the sampling procedure of ground gauges is adequately random. The comparable performance of merged data in training and test gauge groups demonstrated robustness of the merging method on varying gauges. In terms of RSME, CC, and POD, the DBMA-merged data shows much better performance on all gauge groups and elevation bands than the original satellite datasets. The smallest RSME of merged data indicate that the total rainfall amount of the merged data during the evaluation period showed the lowest difference from the total amount of gauged rainfall. The highest CC and POD highlight the best consistency between merged data and

280   ground gauge data on days when most regions in the basin were rainy. The RB of

281   DBMA-merged data is at an intermediate level among the satellite datasets as it is the

282   weighted average of those three datasets. The higher FAR and lower CSI of DBMA-

283   merged data could be attributed to that the merging method detected rainfall events

284   when rainfall estimate is higher than zero in any one of the three satellite datasets and

285   thus resulted in overestimated rainfall occurrence. The overestimated rainfall

286   occurrence might have small effects on the estimation of rainfall amount, as most of

287   the falsely alarmed events were tiny. It is noteworthy that the performance of the

288   merged data shows smaller variance across elevation bands than that of the original

289   satellite datasets. This is most likely benefiting from the spatially dynamic optimal

290   weights for the original satellite data. However, the merged data presented the largest

291   difference from gauged data at the altitudes of 3000-3500 m, because there are much

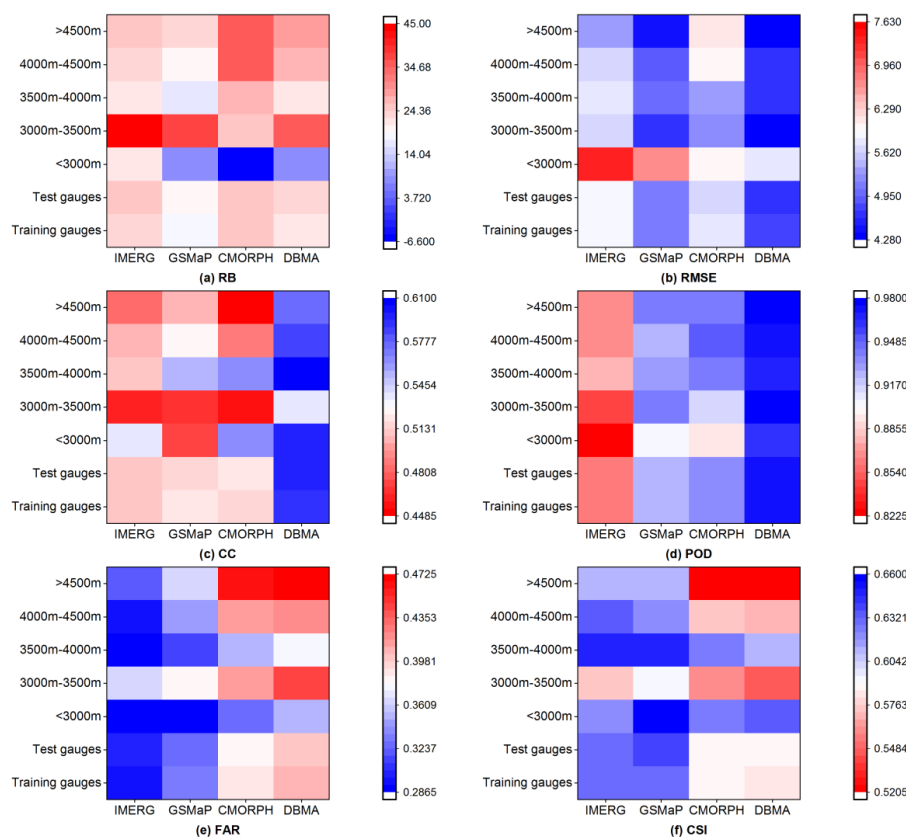292   less gauges on this elevation zone.

Figure 5. Comparisons of the statistical indices of (a) RB, (b)RMSE, (c) CC, (d) POD, (e) FAR
and (f) CSI for training gauges, test gauges and all gauges at five elevation bands.

Figure 6 shows CC of different datasets on specific gauges. The merged data presents higher CC values in regions where are densely gauged, i.e., the middle reaches of YZRB and the east part of the study region, which can be expected as the dense ground gauges provided strongly informative benchmark likelihoods for the estimation of satellite data weights. On most of the gauges (Figure 6a), the merged-data presented higher CC values than the IMERG data, which is consistent with Figure 5c. On contrary, the merged-data showed reduced CC than GSMaP and CMORPH on more gauges (Figures 6b-c), indicating that involving IMERG data in the merging procedure on these gauges lead to deteriorated consistence performance.
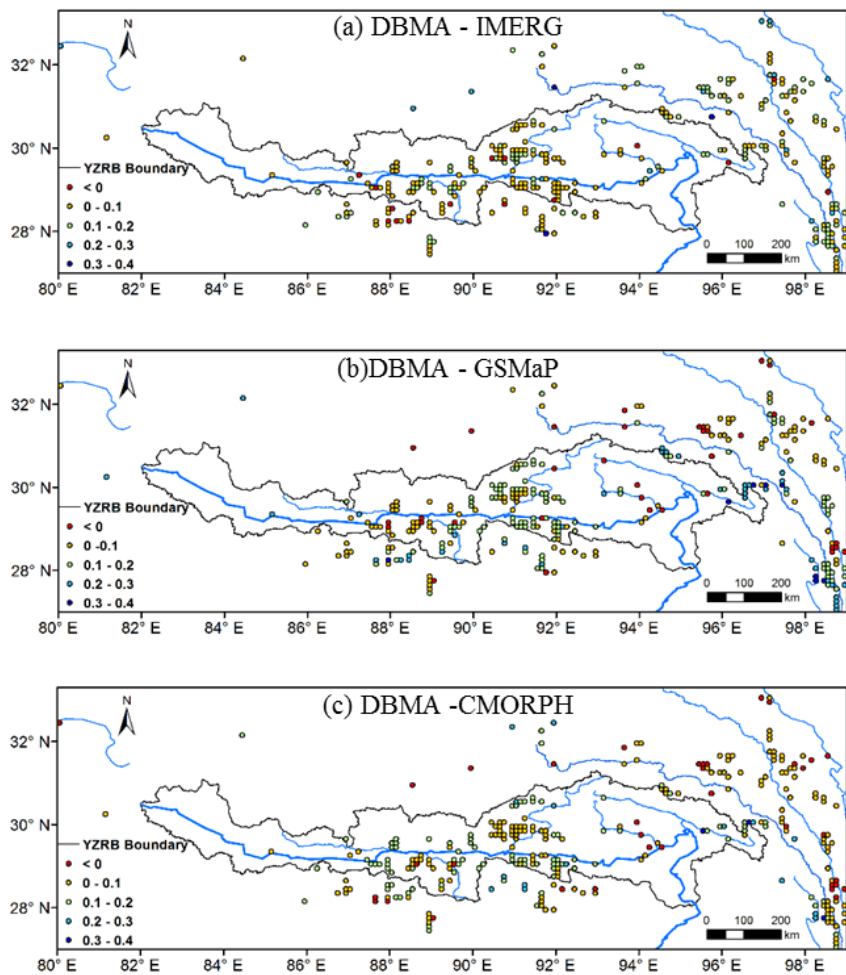
305

Figure 6. Spatial distributions of CC difference between (a) DBMA and IMERG, (b) DBMA and

GSMaP, (c) DBMA and CMORPH

308 **4.3. Hydrological Evaluation**

309 (a) Hydrological simulation

310   Performance of the THREW model forced by different rainfall datasets are

311 compared in Table 4. The DBMA-merged dataset achieved the best runoff simulation

312 among all rainfall inputs, with NSE reaching 0.93 and 0.86 in calibration and validation

313 period, respectively, indicating an excellent agreement between simulated and observed

17

314 hydrographs. Both IMERG and GSMaP underestimated the measured daily discharge,

315 but the DBMA-merged dataset improved such underestimations (see *RB* values in Table

316 4).

317 Table 4. Evaluation metrics of hydrological simulations forced by IMERG, GSMaP, CMORPH

318 and DBMA.

Parameters	IMERG	GSMaP	CMORPH	DBMA
NSEcal	0.91	0.90	0.90	0.93
NSEval	0.75	0.57	0.81	0.86
RB	-0.07	-0.10	0.02	-0.05

319 (b) Uncertainty analysis

320 The automatic algorithm pySOT was ran 200 times to investigate the modelling

321 uncertainty caused by parameter calibration. Figure 7 presents the distributions of *NSE*

322 values estimated by the ensemble parameter sets of the merged and original rainfall

323 forces. It is shown that streamflow simulated by the DBMA data at the Nuxia station

324 presented higher NSEs and smaller uncertainty ranges than that simulated by the

325 original satellite datasets, indicating that streamflow simulations driven by the merged

326 dataset showed stronger robustness and were less affected by uncertainty of parameter

327 calibration.

328 In addition to the Nuxia hydrological station, model performance on simulating

329 streamflow at the interior hydrological stations of Yangcun, Nugesha, Gongbujiangda

330 and Lhasa (Figure 1) were evaluated in Figure 7. It shows that the IMERG forced

331 simulations presented poor NSE outliers lower than zero at the Lhasa station, in spite

332 of their good performance at the Yangcun and Nugesha stations; the GSMaP forced

333 simulations presented large uncertainty ranges in calibration period at Nugesha and

334 Lhasa, and in validation period at Nuxia and Gongbujiangda; the CMORPH forced

335 simulations showed the worst performance in validation period at the interior

336 hydrological stations, despite their sound good performance in calibration period at

337 Yangcun and Nugesha. In comparison to the satellite datasets, the DBMA forced

338 simulations tend to perform consistently better with smaller uncertainties at all the

339   hydrological stations, which can be attributed to that the merged data incorporated the

340   advantages of different datasets in different regions and temporal periods and thus

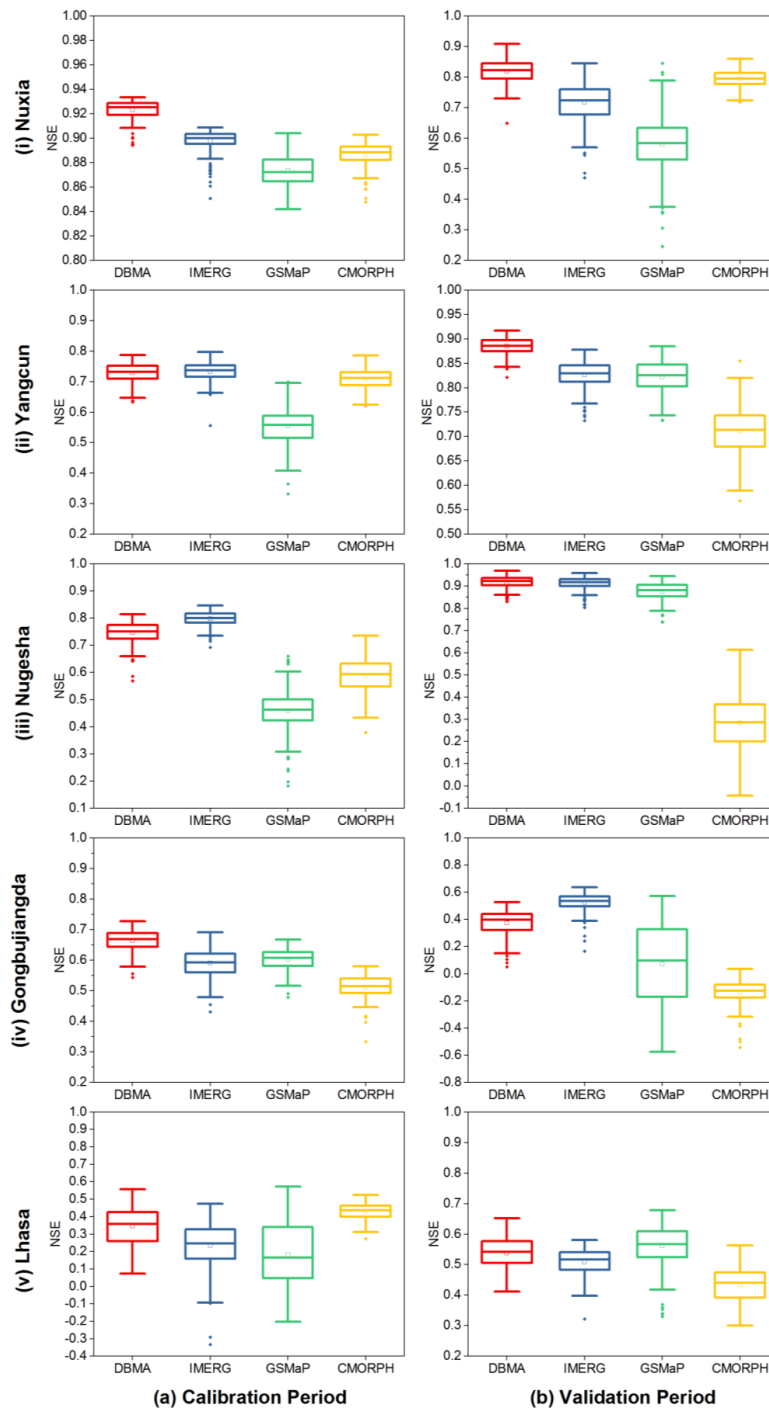341   better captured the spatial variability of rainfall inputs in sub-basins.

Figure 7. Runoff simulations at Nuxia, Yangcun, Nugesha, Gongbujiangda and Lhasa stations

forced by multiple rainfall inputs.

4.4. Comparisons with other datasets

To avoid interference of ground gauge data that merged in the DBMA dataset, the ETC method introduced in Section 3.2 was applied to compare the three merged datasets in Table 5. The RMSE and CC of DBMA calculated by ETC were 1.11 and 0.80, respectively, both of which are obviously superior compared to the corresponding values estimated by CHIRPS and MSWEP, indicating that DBMA data is closer to the true value of rainfall in the study region.

Table 5. Statistical RMSE and CC of merged datasets calculated by the ETC method.

Datasets	DBMA	CHIRPS	MSWEP
RMSE-ETC	1.11	7.15	2.82
CC-ETC	0.80	0.28	0.62

Runoff simulations forced by the three merged datasets during June 10th 2014 to October 31st 2019 estimated by the corresponding optimal parameter sets were presented in Figure 8. Note that the daily runoff is normalized as Eq. 8 for data security reasons. Simulation by the CHIRPS data presented the lowest performance with NSE values of 0.75 and 0.78 in the calibration and validation periods, respectively. The DBMA forced simulation showed the highest performance with NSE values of 0.93 and 0.86 in the calibration and validation periods, followed by the MSWEP forced simulation which estimated NSE values of 0.9 in the calibration period and 0.76 in the validation period. The performance of streamflow forced by the merged datasets are consistent with the agreements between the merged rainfall estimates and ground truth shown in Table 5.

$$Q_{Normalized}^n = \frac{Q_{sim}^n - \min(Q_{obs})}{\max(Q_{obs}) - \min(Q_{obs})} \tag{8}$$
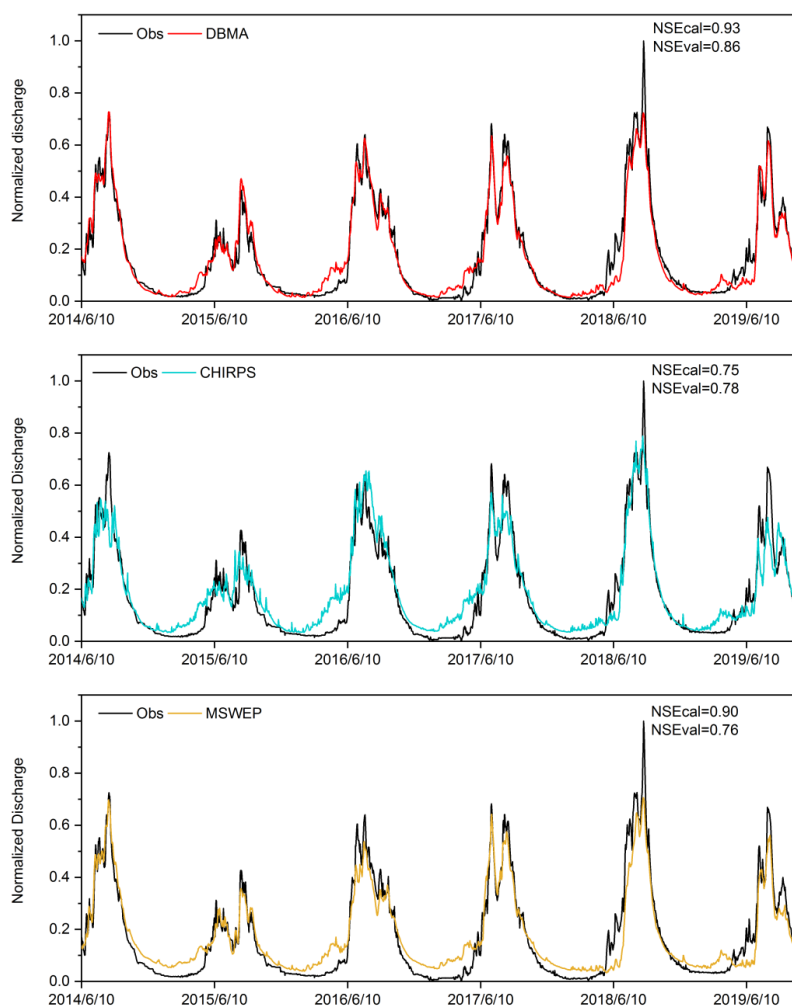
364

365   Figure 8. Simulated daily runoff at Nuxia station forced by DBMA, CHIRPS, and MSWEP.

5 Data Availability

366

367   The high-accuracy rain dataset by merging multi-satellite and dense ground

368   gauges over southern Tibetan Plateau for the warm seasons in 2014-2019 is freely

369   accessible   at   the   National   Tibetan   Plateau   Data   Center

370   https://doi.org/10.11888/Hydro.tpdc.271303 (Li et al.,2021).

6. Summary

We collated ground-based rainfall observations from a dense gauge network over southern TP. The gauged data provides crucial ground references of measured rainfall. Based on this rain gauge network and three satellite rainfall datasets of IMERG, GSMaP, and CMORPH, a merged rainfall dataset in six warm seasons from June 10th to October 31st during 2014-2019 over the southern TP was established. The DBMA method was used to estimate weights varying in space and time of the three satellite datasets for the merged data. The merged rainfall dataset presented improved performance on representing the total amount of rainfall and detecting the occurrence of gauged rainfall events, and provide a more reliable forcing for hydrological simulations in the YZRB, compared to the original satellite datasets. Comparisons with previous merged rainfall datasets of CHIRPS v2.0 and MSWEP v2 that used relatively sparse rain gauges in the study area demonstrated high values of the newly installed rain gauges for providing robust ground reference for the merging of current satellite datasets. Our results indicated that the merged datasets can meet the critical needs of accurate forcing inputs for the simulations of warm season floods and the robustness calibration of hydrological models.

Author contribution

TF and LK designed the research. LK, XR, MY developed the approach and datasets. LK downloaded the datasets and performed most of the computation and analysis work. YL, HZ, LH and MY contributed to the revising of the paper.

Competing interests

The authors declare that they have no conflict of interest.

Earth System
Science
Data

Open Access

Discussions

399   **References**

400   Anagnostou, E. N., & Zhang, X. (2019). Evaluation of Numerical Weather Model–
401   Based Satellite Precipitation Adjustment in Tropical Mountainous Regions.
402   *Journal of Hydrometeorology*, 20(3), 431-445. doi:10.1175/jhm-d-18-0008.1
403   Beck, H. E., Wood, E. F., Pan, M., Fisher, C. K., Miralles, D. G., van Dijk, A. I. J. M.,
404   Adler, R. F. (2019). MSWEP V2 Global 3-Hourly 0.1° Precipitation: Methodology
405   and Quantitative Assessment. *Bulletin of the American Meteorological Society*,
406   100(3), 473-500. doi:10.1175/bams-d-17-0138.1
407   Becker, A., Finger, P., Meyer-Christoffer, A., Rudolf, B., Schamm, K., Schneider, U.,
408   & Ziese, M. (2013). A description of the global land-surface precipitation data
409   products of the Global Precipitation Climatology Centre with sample applications
410   including centennial (trend) analysis from 1901–present. *Earth System Science
411   Data*, 5(1), 71-99. doi:10.5194/essd-5-71-2013
412   Biskop, S., Maussion, F., Krause, P., & Fink, M. (2016). Differences in the water-
413   balance components of four lakes in the southern-central Tibetan Plateau.
414   *Hydrology and Earth System Sciences*, 20(1), 209-225. doi:10.5194/hess-20-209-
415   2016
416   Bitew, M. M. G., Mekonnen. (2010). Evaluation through independent measurements:

Earth System
Science
Data

Open Access

Discussions

417   Complex terrain and humid tropical region in Ethiopia. In *Satellite rainfall*

418   *applications for surface hydrology* (pp. 205-214): Springer, Dordrecht.

419   Bookhagen, B., & Burbank, D. W. (2006). Topography, relief, and TRMM-derived

420   rainfall variations along the Himalaya. *Geophysical Research Letters*, 33(8).

421   doi:10.1029/2006gl026037

422   David Eriksson, David Bindel, Christine A. Shoemaker. pySOT and POAP: An event-

423   driven asynchronous framework for surrogate optimization. *arXiv* preprint

424   arXiv:1908.00420, 2019.

425   Derin, Y., Anagnostou, E., Anagnostou, M. N., Kalogiros, J., Casella, D., Marra, A. C.,

426   Sano, P. (2018). Passive Microwave Rainfall Error Analysis Using High-

427   Resolution X-Band Dual-Polarization Radar Observations in Complex Terrain.

428   *IEEE Transactions on Geoscience and Remote Sensing*, 56(5), 2565-2586.

429   doi:10.1109/tgrs.2017.2763622

430   Derin, Y., Anagnostou, E., Berne, A., Borga, M., Boudevillain, B., Buytaert, W.,

431   Yilmaz, K. (2019). Evaluation of GPM-era Global Satellite Precipitation Products

432   over Multiple Complex Terrain Regions. *Remote Sensing*, 11(24).

433   doi:10.3390/rs11242936

434   Dinku, T. C., Stephen J.; Ceccato, Pietro. (2010). Comparison of CMORPH and

435   TRMM-3B42 over mountainous regions of Africa and South America. In *Satellite*

436   *rainfall applications for surface hydrology* (pp. 193-204): Springer, Dordrecht.

437   Funk, C., Peterson, P., Landsfeld, M., Pedreros, D., Verdin, J., Shukla, S., Michaelsen,

438   J. (2015). The climate hazards infrared precipitation with stations--a new

439   environmental record for monitoring extremes. *Sci Data*, 2, 150066.

440   doi:10.1038/sdata.2015.66

441   Gao, Y. C., & Liu, M. F. (2013). Evaluation of high-resolution satellite precipitation

442   products using rain gauge observations over the Tibetan Plateau. Hydrology and

443   Earth System Sciences, 17(2), 837-849. doi:10.5194/hess-17-837-2013

444   Goswami, D. C. (1985). Brahmaputra River, Assam, India: Physiography, basin

445   denudation, and channel aggradation. *Water Resources Research*, 21(7), 959-978.

446   He, J., Yang, K., Tang, W., Lu, H., Qin, J., Chen, Y., & Li, X. (2020). The first high-
447   resolution meteorological forcing dataset for land process studies over China.
448   Scientific data, 7(1), 1-11.

449   He, Z., Yang, L., Tian, F., Ni, G., Hou, A., & Lu, H. (2017). Intercomparisons of
450   Rainfall Estimates from TRMM and GPM Multisatellite Products over the Upper
451   Mekong River Basin. *Journal of Hydrometeorology*, 18(2), 413-430.
452   doi:10.1175/jhm-d-16-0198.1

453   Hong, Y., Gochis, D., Cheng, J.-t., Hsu, K.-l., & Sorooshian, S. (2007). Evaluation of
454   PERSIANN-CCS Rainfall Measurement Using the NAME Event Rain Gauge
455   Network. *Journal of Hydrometeorology*, 8(3), 469-482. doi:10.1175/jhm574.1

456   Hou, A. Y., Kakar, R. K., Neeck, S., Azarbarzin, A. A., Kummerow, C. D., Kojima, M.,
457   Iguchi, T. (2014). The Global Precipitation Measurement Mission. *Bulletin of the
458   American Meteorological Society*, 95(5), 701-722. doi:10.1175/bams-d-13-
459   00164.1

460   Hou, S., Tian, F., Yang, L., Hu, H., & Hou, A. (2018). How Does the Evaluation of the
461   GPM IMERG Rainfall Product Depend on Gauge Density and Rainfall Intensity?
462   *Journal of Hydrometeorology*, 19(2), 339-349. doi:10.1175/jhm-d-17-0161.1

463   Huang, J., Kang, S., Zhang, Q., Jenkins, M. G., Guo, J., Zhang, G., & Wang, K. (2012).
464   Spatial distribution and magnification processes of mercury in snow from high-
465   elevation glaciers in the Tibetan Plateau. *Atmospheric Environment*, 46, 140-146.
466   doi:10.1016/j.atmosenv.2011.10.008

467   Immerzeel, W. W., Van Beek, L. P., & Bierkens, M. F. (2010). Climate change will
468   affect the Asian water towers. Science, 328(5984), 1382-1385.

469   Jiang, S., Ren, L., Hong, Y., Yong, B., Yang, X., Yuan, F., & Ma, M. (2012).
470   Comprehensive evaluation of multi-satellite precipitation products with a dense
471   rain gauge network and optimally merging their simulated hydrological flows
472   using the Bayesian model averaging method. Journal of Hydrology, 452-453, 213-

473   225. doi:10.1016/j.jhydrol.2012.05.055

474   Joyce, R. J., JE; Arkin, PA; Xie, PP. (2004). CMORPH: A Method that Produces Global

475   Precipitation Estimates from Passive Microwave and Infrared Data at High Spatial

476   and Temporal Resolution. *Journal of Hydrometeorology*, 5(3), 487-503.

477   Kidd, C., & Levizzani, V. (2011). Status of satellite precipitation retrievals. *Hydrology*

478   *and Earth System Sciences*, 15(4), 1109-1116. doi:10.5194/hess-15-1109-2011

479   Kumar, V., Jain, S. K., & Singh, Y. (2010). Analysis of long-term rainfall trends in India.

480   *Hydrological   Sciences   Journal*,   55(4),   484-496.

481   doi:10.1080/02626667.2010.481373

482   Liu, J., Shangguan, D., Liu, S., Ding, Y., Wang, S., & Wang, X. (2019). Evaluation and

483   comparison of CHIRPS and MSWEP daily-precipitation products in the Qinghai-

484   Tibet Plateau during the period of 1981–2015. Atmospheric Research, 230.

485   doi:10.1016/j.atmosres.2019.104634

486   Lu, D., & Yong, B. (2018). Evaluation and Hydrological Utility of the Latest GPM

487   IMERG V5 and GSMaP V7 Precipitation Products over the Tibetan Plateau.

488   Remote Sensing, 10(12). doi:10.3390/rs10122022

489   Ma, Y., Hong, Y., Chen, Y., Yang, Y., Tang, G., Yao, Y., Liu, R. (2018). Performance of

490   Optimally Merged Multisatellite Precipitation Products Using the Dynamic

491   Bayesian Model Averaging Scheme Over the Tibetan Plateau. *Journal of*

492   *Geophysical   Research: Atmospheres*,   123(2),   814-834.

493   doi:10.1002/2017jd026648

494   McColl, K. A., Vogelzang, J., Konings, A. G., Entekhabi, D., Piles, M., & Stoffelen, A.

495   (2014). Extended triple collocation: Estimating errors and correlation coefficients

496   with respect to an unknown target. *Geophysical Research Letters*, 41(17), 6229-

497   6236. doi:10.1002/2014gl061322

498   Nash, J. E., & Sutcliffe, J. V. (1970). River flow forecasting through conceptual models

499   part I—A discussion of principles. *Journal of hydrology*, 10(3), 282-290.

500   Parsons, D. B., Rasmussen, R. M., Dai, A., & Trenberth, K. E. (2003). The Changing

501   Character of Precipitation. *Bulletin of the American Meteorological Society*, 84(9),

502   1205-1218. doi:10.1175/bams-84-9-1205

503   Ren, Z. H., Zhao, P., Zhang, Q., Zhang, Z. F., Cao, L. J., Yang, Y. R., & Chen, Z. (2010).

504   Quality control procedures for hourly precipitation data from automatic weather

505   stations in China. *Meteorol. Mon*, 36(7), 123-132.

506   Roebeling, R. A., Wolters, E. L. A., Meirink, J. F., & Leijnse, H. (2012). Triple

507   Collocation of Summer Precipitation Retrievals from SEVIRI over Europe with

508   Gridded Rain Gauge and Weather Radar Data. *Journal of Hydrometeorology*,

509   13(5), 1552-1566. doi:10.1175/jhm-d-11-089.1

510   Stoffelen, A. (1998). Toward the true near-surface wind speed: Error modeling and

511   calibration using triple collocation. *Journal of Geophysical Research: Oceans*,

512   103(C4), 7755-7766. doi:10.1029/97jc03180

513   Su, Y., Zhao, C., Wang, Y., & Ma, Z. (2020). Spatiotemporal Variations of Precipitation

514   in China Using Surface Gauge Observations from 1961 to 2016. Atmosphere,

515   11(3). doi:10.3390/atmos11030303

516   Sun, R., Yuan, H., Liu, X., & Jiang, X. (2016). Evaluation of the latest satellite–gauge

517   precipitation products and their hydrologic applications over the Huaihe River

518   basin. Journal of Hydrology, 536, 302-319. doi:10.1016/j.jhydrol.2016.02.054

519   Tang, G., Ma, Y., Long, D., Zhong, L., & Hong, Y. (2016). Evaluation of GPM Day-1

520   IMERG and TMPA Version-7 legacy products over Mainland China at multiple

521   spatiotemporal scales. Journal of Hydrology, 533, 152-167.

522   doi:10.1016/j.jhydrol.2015.12.008

523   Tang, G., Clark, M. P., Papalexiou, S. M., Ma, Z., & Hong, Y. (2020). Have satellite

524   precipitation products improved over last two decades? A comprehensive

525   comparison of GPM IMERG with nine satellite and reanalysis datasets. Remote

526   Sensing of Environment, 240. doi:10.1016/j.rse.2020.111697

527   Tong, K., Su, F., Yang, D., & Hao, Z. (2014). Evaluation of satellite precipitation

528   retrievals and their potential utilities in hydrologic modeling over the Tibetan

Earth System
Science
Data

529   Plateau. Journal of Hydrology, 519, 423-437. doi:10.1016/j.jhydrol.2014.07.044

530   Tian, F., Hu, H., Lei, Z., & Sivapalan, M. (2006). Extension of the Representative

531   Elementary Watershed approach for cold regions via explicit treatment of energy

532   related processes. *Hydrology and Earth System Sciences*, 10(5), 619-644.

533   Ushio, T., Sasashige, K., Kubota, T., Shige, S., Okamoto, K. i., Aonashi, K., Kawasaki,

534   Z.-I. (2009). A Kalman Filter Approach to the Global Satellite Mapping of

535   Precipitation (GSMaP) from Combined Passive Microwave and Infrared

536   Radiometric Data. *Journal of the Meteorological Society of Japan*, 87A, 137-151.

537   doi:10.2151/jmsj.87A.137

538   Wang, Y., Wang, L., Li, X., Zhou, J., & Hu, Z. (2020). An integration of gauge, satellite,

539   and reanalysis precipitation datasets for the largest river basin of the Tibetan

540   Plateau. *Earth System Science Data*, 12(3), 1789-1803. doi:10.5194/essd-12-

541   1789-2020

542   Wang, Z., Zhong, R., Lai, C., & Chen, J. (2017). Evaluation of the GPM IMERG

543   satellite-based precipitation products and the hydrological utility. Atmospheric

544   Research, 196, 151-163. doi:10.1016/j.atmosres.2017.06.020

545   Wilks, D. S. (2011). Statistical methods in the atmospheric sciences (Vol. 100).

546   Academic press.

547   Wolff, D. B., Nelkin, E. J., Bolvin, D. T., Huffman, G. J., Adler, R. F., Gu, G., Stocker,

548   E. F. (2007). The TRMM Multisatellite Precipitation Analysis (TMPA): Quasi-

549   Global, Multiyear, Combined-Sensor Precipitation Estimates at Fine Scales.

550   *Journal of Hydrometeorology*, 8(1), 38-55. doi:10.1175/jhm560.1

551   Xu, R., Tian, F., Yang, L., Hu, H., Lu, H., & Hou, A. (2017). Ground validation of GPM

552   IMERG and TRMM 3B42V7 rainfall products over southern Tibetan Plateau

553   based on a high-density rain gauge network. *Journal of Geophysical Research:*

554   *Atmospheres*, 122(2), 910-924. doi:10.1002/2016jd025418

555   Xue, X., Hong, Y., Limaye, A. S., Gourley, J. J., Huffman, G. J., Khan, S. I., Chen, S.

556   (2013). Statistical and hydrological evaluation of TRMM-based Multi-satellite

557   Precipitation Analysis over the Wangchu Basin of Bhutan: Are the latest satellite

558   precipitation products 3B42V7 ready for use in ungauged basins? *Journal of*

559   *Hydrology*, 499, 91-99. doi:10.1016/j.jhydrol.2013.06.042

560 Yang, D., Li, Z., Gao, B., Jiao, Y., Hong, Y., & Xu, T. (2015). Multiscale Hydrologic

561   Applications of the Latest Satellite Precipitation Products in the Yangtze River

562   Basin using a Distributed Hydrologic Model. *Journal of Hydrometeorology*, 16(1),

563   407-426. doi:10.1175/jhm-d-14-0105.1

564 Yang, S., Chen, M., Xie, P., Yatagai, A., Hayasaka, T., Fukushima, Y., & Liu, C. (2007).

565   A Gauge-Based Analysis of Daily Precipitation over East Asia. *Journal of*

566   *Hydrometeorology*, 8(3), 607-626. doi:10.1175/jhm583.1

567 Yao, T., Thompson, L. G., Mosbrugger, V., Zhang, F., Ma, Y., Luo, T., & Fayziev, R.

568   (2012). Third pole environment (TPE). *Environmental Development*, 3, 52-64.

569 Yilmaz, K. K., Vergara, H. J., Rodríguez-Sánchez, J.-P., Salerno, F., Sahlu, D.,

570   Nikolopoulos, E. I., Derin, Y. (2016). Multiregional Satellite Precipitation

571   Products Evaluation over Complex Terrain. *Journal of Hydrometeorology*, 17(6),

572   1817-1836. doi:10.1175/jhm-d-15-0197.1

573 Yong, B., Chen, B., Gourley, J. J., Ren, L., Hong, Y., Chen, X., Gong, L. (2014).

574   Intercomparison of the Version-6 and Version-7 TMPA precipitation products over

575   high and low latitudes basins with independent gauge networks: Is the newer

576   version better in both real-time and post-real-time analysis for water resources and

577   hydrologic extremes? *Journal of Hydrology*, 508, 77-87.

578   doi:10.1016/j.jhydrol.2013.10.050

579 Yong, B., Hong, Y., Ren, L.-L., Gourley, J. J., Huffman, G. J., Chen, X., Khan, S. I.

580   (2012). Assessment of evolving TRMM-based multisatellite real-time

581   precipitation estimation methods and their impacts on hydrologic prediction in a

582   high latitude basin. *Journal of Geophysical Research: Atmospheres*, 117(D9), n/a-

583   n/a. doi:10.1029/2011jd017069

584 Zhai, P., Zhang, X., Wan, H., & Pan, X. (2005). Trends in total precipitation and

585   frequency of daily precipitation extremes over China. Journal of climate, 18(7),

586   1096-1108.

587   Zhao, Y., Zhu, J., & Xu, Y. (2014). Establishment and assessment of the grid

588   precipitation datasets in China for recent 50 years. J. Meteor. Sci, 34(4), 414-420.